Energy 33 (2008) 1277–1287

Contents lists available at ScienceDirect

Energy

journal homepage: www.elsevier.com/locate/energy

Heat transfer and friction factor correlations for a duct having dimple-shape artificial roughness for solar air heaters

R.P. Saini *, Jitendra Verma

Alternate Hydro Energy Centre, Indian Institute of Technology Roorkee, Uttarakhand 247667, India

ARTICLE INFO

Article history:
Received 26 June 2007

Keywords:
Artificial roughness
Solar air heater
Nusselt number
Friction factor

ABSTRACT

The heat transfer coefficient between the absorber plate and air can be considerably increased by using artificial roughness on the underside of the absorber plate of a solar air heater duct. Under the present work, an experimental study has been carried out to investigate the effect of roughness and operating parameters on heat transfer and friction factor in a roughened duct provided with dimple-shape roughness geometry. The investigation has covered the range of Reynolds number (Re) from 2000 to 12,000, relative roughness height (e/D) from 0.018 to 0.037 and relative pitch (p/e) from 8 to 12. Based on the experimental data, values of Nusselt number (Nu) and friction factor (f_r) have been determined for different values of roughness and operating parameters. In order to determine the enhancement in heat transfer and increment in friction factor values of Nusselt number and friction factor have been compared with those of smooth duct under similar flow conditions. Correlations for Nusselt number and friction factor have been developed for solar air heater duct provided such artificial roughness geometry.

1. Introduction

Several investigators have investigated forced convection heat transfer in smooth and roughened ducts, and lots of useful information is available in the literature. The use of artificial roughness on a surface is an effective technique to enhance heat transfer to fluid flowing in ducts. Artificial roughness can be provided by fixing wires, ribs, wire mesh or expanded metal mesh and by providing roughness in dimple-shape geometry. Several investigations have been carried out to study the effect of artificial roughness on heat transfer and friction factor for two opposite roughened surfaces by Han [1,2], Han et al. [3–5], Lau et al. [6–8], Taslim et al. [9,10], Liou and Hwang [11], Han and Park [12] and correlations for heat transfer coefficient and friction factor were developed by these investigators. Prasad and Mullick [13], Gupta [14], Saini and Saini [15], Karwa [16], Jaurker et al. [17], Bhagoria et al. [18], Chaube et al. [19], Verma and Prasad [20] and Gupta et al. [21] have carried out investigations on rib-roughened absorber plates of solar air heaters that form a system with only one roughened wall and three smooth walls. Correlations for heat transfer coefficient and friction factor have been developed for such systems. Mittal et al. [22] compared the effective efficiency of the solar air heater having different types of roughness elements on the absorber plate. A review on roughness geometries used in solar air heater ducts was presented by Varun et al. [23].

The application of artificial roughness in the form of dimples on the heat transfer surface may be attractive roughness geometry in solar air heater ducts as it does not require complicated manufacturing process, particularly if the dimple shape is a spherical indentation. Because of this characteristic, dimples do not add extra weight to the absorbing plate, especially if surface material is removed to form the dimples. On thinner materials, an indentation-producing device can be used to form the dimples, which then gives protrusions on the opposite side. This then leads to another advantage because substantial heat transfer augmentations are also provided by the array of protrusions. A number of investigations have been carried out on the heat transfer characteristics of channels or pipes with dimple roughness on the surface. Schukin et al. [24] studied the effects of channel geometry (converging and diverging channels) on heat transfer for downstream flow over a single hemispherical cavity. Chyu et al. [25] reported overall heat transfer rate as 2.5 times more in case of duct having dimple-shape roughness geometry than that of a smooth surface. Lin et al. [26] presented corresponding flow and heat transfer predictions in order to explain the observed heat transfer behavior. Moon et al. [27] investigated the effect of channel height on the heat transfer and friction in a dimpled passage. Heat transfer enhancement of the order of 2.0 and pressure drop penalties of the order of 1.6–2.0 times over smooth

* Corresponding author. Tel.: +91 1332 285841; fax: 91 1332 273517.
E-mail address: rajsafah@iitr.ernet.in (R.P. Saini).

0360-5442/$ - see front matter © 2008 Elsevier Ltd. All rights reserved.
doi:10.1016/j.energy.2008.02.017

Nomenclature

A	area of the flow (m^2)
A_T	throat area of the orifice (m^2)
A_C	area of the absorber plate (m^2)
C_d	coefficient of discharge for the orifice meter
C_P	specific heat of air (kJ/kg/K)
D	equivalent diameter of the duct (m) ($= 2WH/(W+H)$)
e	height of the roughness element (m)
ΔF	pressure drop across the test section (N/m^2)
f_r	friction factor for roughened absorber plates
f_s	friction factor for the smooth absorber plate
H	height of the duct (m)
$\bar{h}$	average heat transfer coefficient ($W/m^2/K$)
k	thermal conductivity of air (W/m/K)
L	length of the collector (m)
m	mass flow rate (kg/s)
Nu	Nusselt number for the roughened duct
Nu_s	Nusselt number for the smooth duct
p	roughness pitch (m)
Pr	Prandtl number
ΔP	pressure drop across the orifice meter (N/m^2)
R_{av}	average radial distance of the duct
Re	Reynolds number
W	width of the duct (m)
β	diameter ratio, D_2/D_1
θ	tilt angle of the manometer
ρ	density of fluid (kg/m^3)
ν	kinematic viscosity of fluid (m^2/s)
t_i	inlet temperature of air (°C)
t_o	outlet temperature of air (°C)
$\bar{t}_a$	average temperature of air (°C)
$\bar{t}_p$	average temperature of the absorbing plate (°C)

surfaces were reported. Mahmood et al. [28] carried out a detailed flow and heat transfer study on a dimpled plate and identified specific vortex structures responsible for augmenting heat transfer from the downstream rims of each dimple. Heat transfer enhancement ranging from 1.8 to 2.4 times over smooth plates was observed. Investigations made by various investigators [25–28] have been for heat transfer and friction characteristics in ducts for the flow of high Reynolds number. The range of Reynolds number investigated by them is not suitable for the airflow in solar air heater ducts. Further most of the investigations made so far in rectangular ducts were having more than 1 roughened surface walls provided with such artificial roughness geometry.

The present investigation was, therefore, carried out with the objective of extensive experimentation on dimple-shape geometry as artificial roughness provided on to the underside of one broad wall of the duct of a solar air heater, in order to collect data on heat transfer and fluid flow characteristics. The experimental data are presented in the form of Nusselt number and friction factor plots as function of Reynolds number for different roughness parameters. Using experimental data collected during extensive experimental study, correlations for Nusselt number and friction factor have also been developed.

2. Experimental program

2.1. Experimental setup

A schematic diagram of the experimental setup including the test section is shown in Fig. 1. The flow system consisted of an entry section, a test section, an exit section, a flow meter and an air blower. The duct having the dimensions of inner cross-section as 2400 mm × 300 mm × 25 mm was made of wooden panels. The test section having a length of 1000 mm was provided. The length of entry and exit section was provided as 900 mm and 500 mm, respectively. These lengths were taken as per ASHRAE Standard 93–97 [29]. An electric heater having a size of 1500 mm × 290 mm was fabricated by combining series and parallel loops of heating wire on a 5-mm-thick asbestos sheet. A mica sheet of 1 mm thick was placed on the electric heater wire, in order to get uniform radiation between the electric heater and absorber plate. The heat flux may be varied from 0 to 1000 W/m^2 with the help of a variac connected across it. A 50 mm thick layer of glass wool as an insulating material and a 12 mm thick wooden panel was provided in order to minimize the heat losses from the topside of the heater assembly. A 4-mm-thick galvanized iron (GI) sheet having roughened surface on its under side was provided as heat absorber plate. This plate formed the top wall of the duct. Fig. 2 shows the cross-section of the duct. The top of the entry and exit sections of the duct was covered with 8-mm-thick wooden panels. In order to ensure that no heat losses occur due to conduction effect, the duct was insulated properly by providing glass wool at the outer surface of the duct covering entry length, test length and exit length.

The mass flow rate of air was measured by means of a calibrated orifice meter connected with an inclined manometer. Control valves were provided in the flow lines to control the flow. An orifice meter plate was designed for the flow measurement in the pipe having inner diameter of 80 mm. Calibrated copper–constantan thermocouples were used to measure the temperature of air and absorbing plate temperature at different locations. A digital micro-Volt-millimeter was used to indicate the output of the thermocouples. The pressure drop across the test section was measured with the help of a micro-manometer.

2.2. Instrumentations

2.2.1. Temperature measurement

Calibrated copper–constantan thermocouples (24 SWG) with digital micro-Volt-millimeter, indicating output in degree centigrade with an accuracy of 0.1 °C were used to measure air temperature and the temperatures of the absorber plate at different locations. The thermocouples were calibrated with a standard thermometer. Fig. 3 shows the calibration curve for the thermocouples used. Fifteen thermocouples have been pasted on the top surface of the absorber plate to record the plate temperature. The locations of thermocouples are shown in Fig. 4. The temperature of air inside the duct was recorded by 10 thermocouples inserted inside the duct at different locations as shown in Fig. 4. Thermocouple output was measured with the help of a digital micro-Volt-millimeter through a selector switch.

2.2.2. Airflow measurement

The mass flow rate of air was measured by means of a calibrated orifice meter connected with an inclined manometer. The control valves were provided in the line to control the flow. The description of the orifice-meter is shown in Fig. 5. The orifice plate was calibrated with a Pitot tube. The calibration curve of the same is given in Fig. 6.

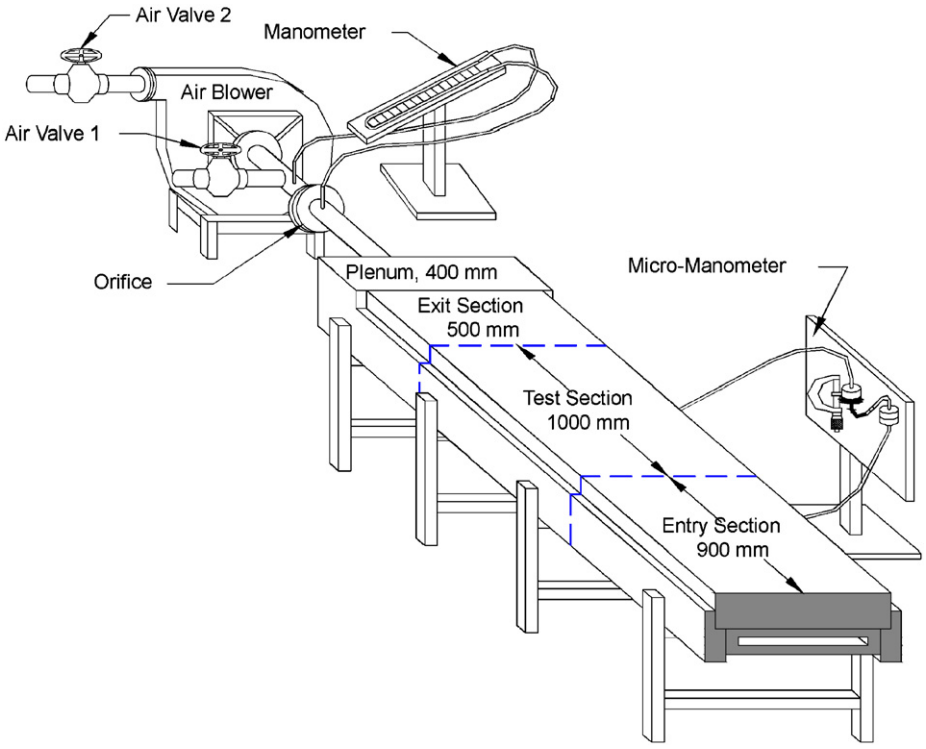

Fig. 1. Schematic diagram of experimental setup.

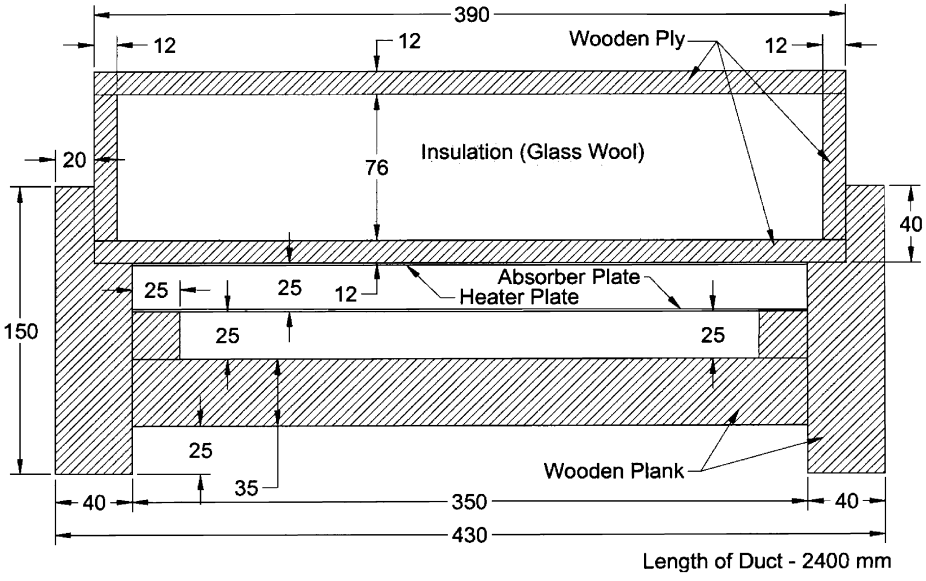

Fig. 2. Cross-section of the duct.

2.2.3. Pressure drop measurement in duct

Pressure drop across the test-section of the duct was measured by means of a micro-manometer having accuracy 0.01 mm. The micro-manometer consisted of a moveable reservoir, a fixed reservoir and an inclined transparent tube connected to these reservoirs through flexible tubes. The movable reservoir was mounted on a sliding arrangement using a micrometer having a least count of 0.01 mm. The movement of reservoir was recorded. The two reservoirs were connected with the air taps of the duct through flexible tubes. The meniscus was maintained at a fixed prescribed mark by moving the reservoir up or down and the movement was noted which yield the pressure difference across the two pressure tapping. The butyl-alcohol having specific gravity 0.8 has been used in the manometer to increase the accuracy further. The locations of the air taps were as shown in Fig. 4.

2.3. Roughness geometry and range of parameters

Fig. 7 shows the roughness geometry of dimple-shape, which has been investigated under the present investigation. The range

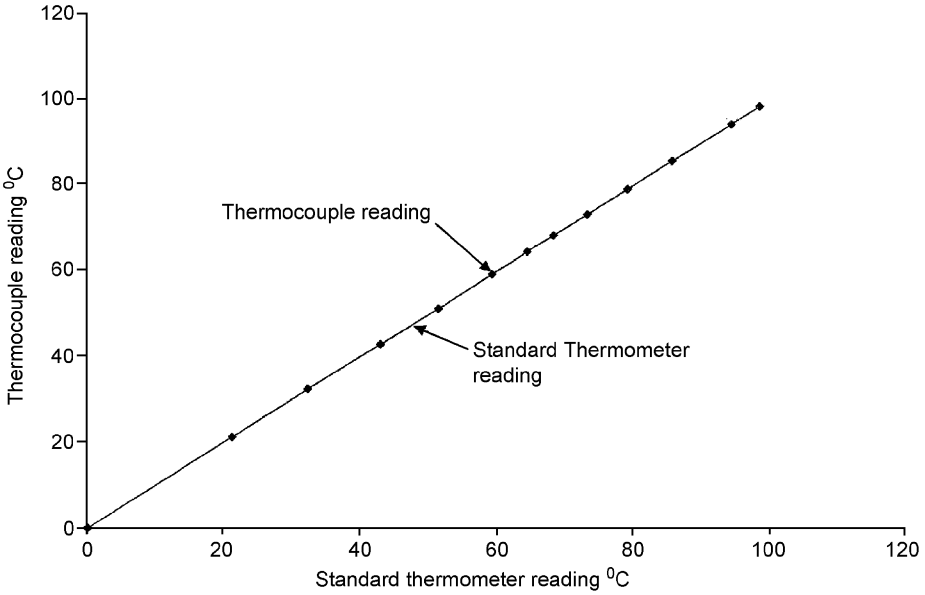

Fig. 3. Calibration curve for thermocouples.

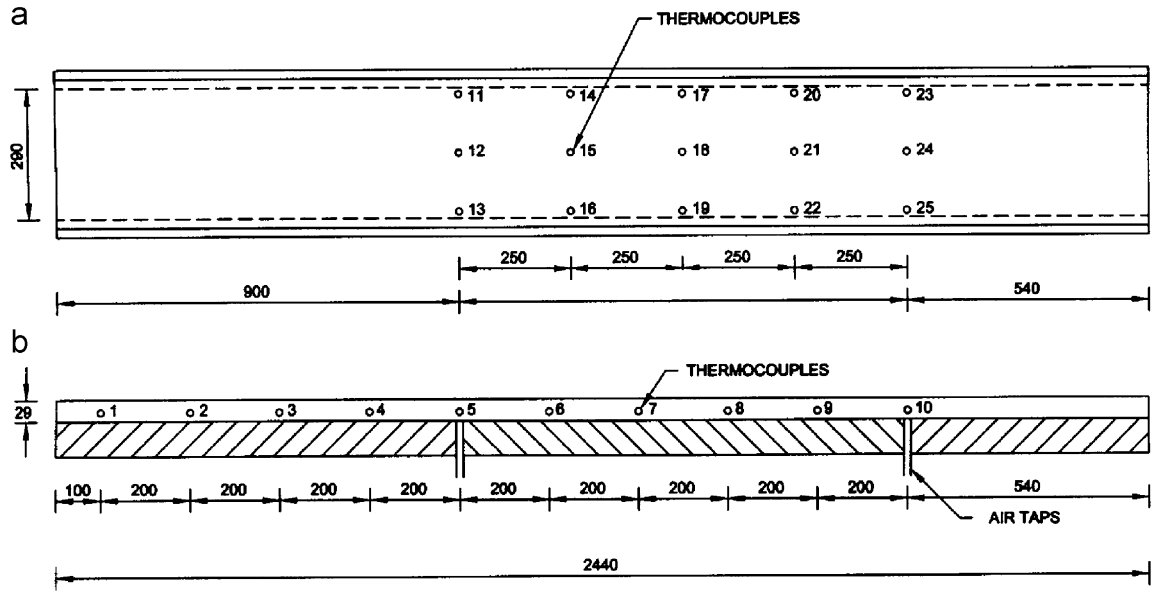

Fig. 4. Location of thermocouple on absorber plate and thermocouple and air taps in air duct.

of parameters covered under the present experimental study is as given below;

(i) Reynolds number $2000 \leqslant Re \leqslant 12{,}000$.
(ii) Relative roughness height $0.0189 \leqslant e/D \leqslant 0.038$.
(iii) Relative roughness pitch $8 \leqslant p/e \leqslant 12$.

3. Experimental procedure

The test runs to collect relevant heat transfer and flow friction data were conducted under steady-state conditions. For different airflow rates, the system was allowed to attain a steady state before the data were recorded. The following parameters were measured.

(i) Temperature of the absorber plate and air at inlet and outlet of the test section.
(ii) Pressure drop across the test section.
(iii) Pressure difference across the orifice meter.

4. Data reduction

Steady-state values of the plate and air temperature in the duct at various locations were used to determine the values of useful parameters. Mass flow rate, m, velocity of air, v, heat supplied to the air, q and heat transfer coefficient, h, were calculated by using following expressions:

$$m = C_d A_T \left[\frac{2\rho \Delta P \sin\theta}{1-\beta^4}\right]^{1/2} \tag{1}$$

$$v = \frac{m}{\rho W H} \tag{2}$$

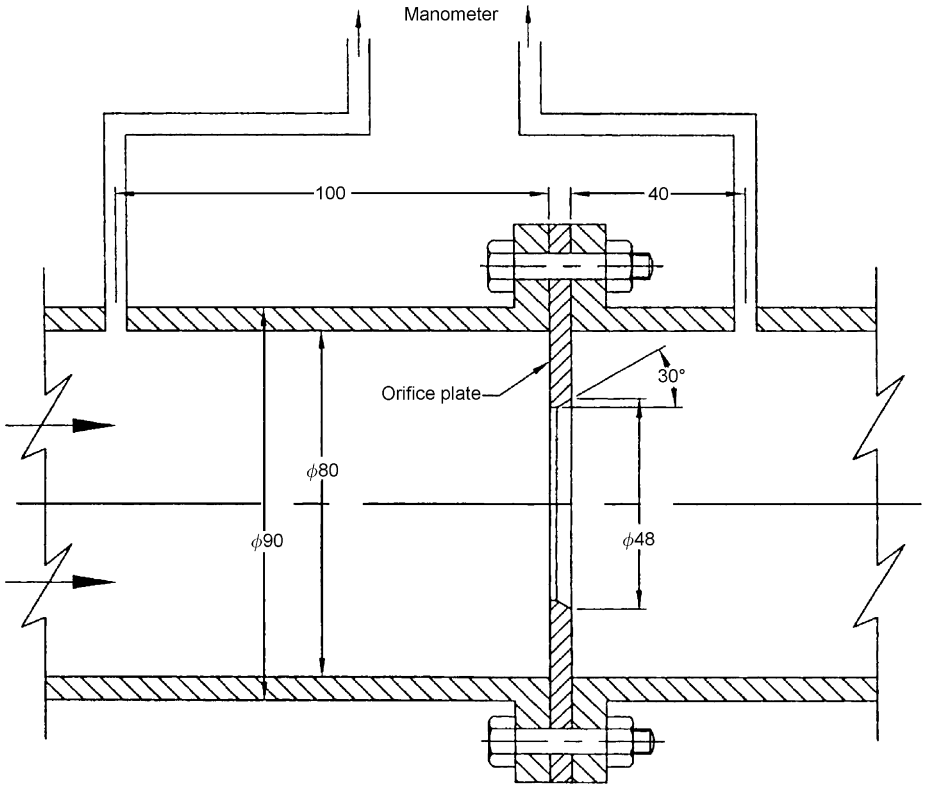

Fig. 5. Description of the orifice-meter.

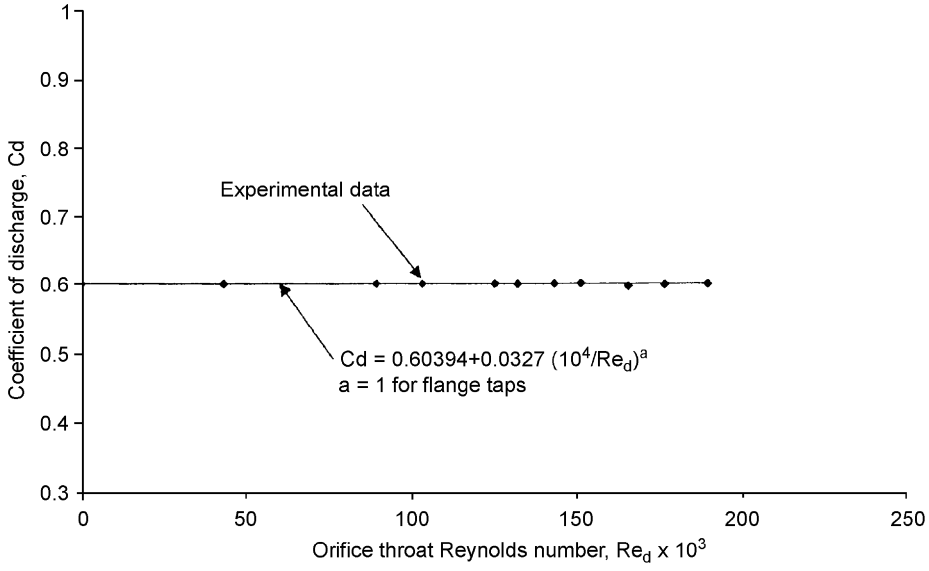

Fig. 6. Calibration curve of the orifice-meter.

$$q = mC_p(t_o - t_i) \tag{3}$$

$$\bar{h} = \frac{mC_p(t_o - t_i)}{A_C(\bar{t}_p - \bar{t}_a)} \tag{4}$$

where the temperature $\bar{t}_p$ and $\bar{t}_a$ are average values of the absorber plate and fluid (air) temperature, respectively. The average value of plate temperature ($\bar{t}_p$) was determined from the detailed temperature profile of the absorbing plate. It was found that the temperature of the absorber plate varies predominantly in the flow direction only and is linear. The variations in the direction normal to the flow were found to be negligible. The plate temperature was determined at 15 locations on the plate as shown in Fig. 4. The average plate temperature ($\bar{t}_p$) was determined by taking average temperature of 15 thermocouples located at different locations as shown in Fig. 4.

The air temperature variations were found to be linear. Since the temperature variations of the absorber plate in the direction normal to the flow were found to be negligible in that direction, the air temperature variations in that direction can be assumed to be negligible. The temperature variation in the direction normal to the absorber plate could not be measured because of very small

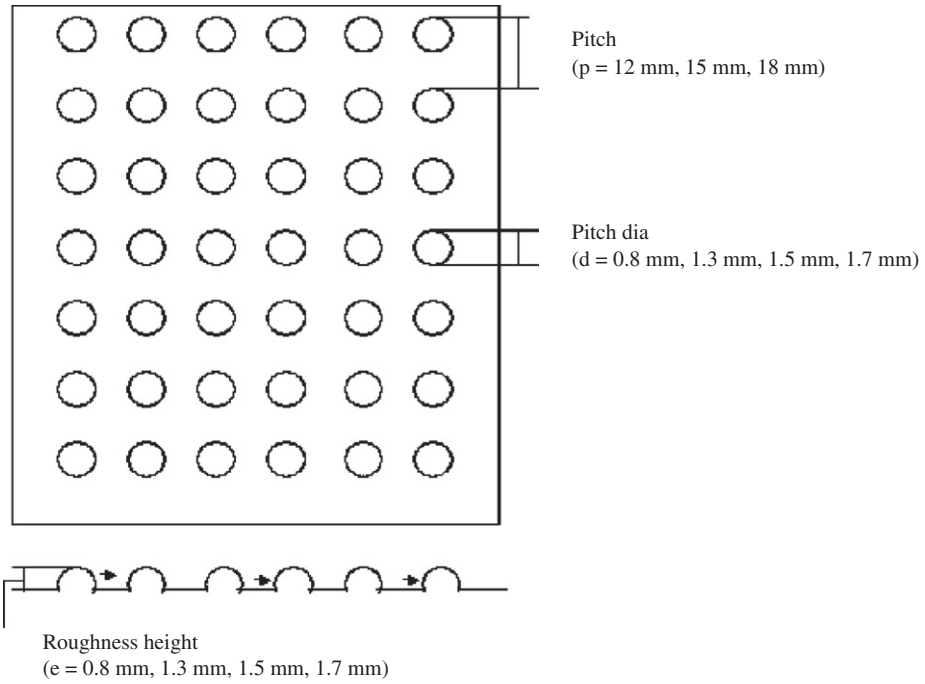

Fig. 7. Schematic diagram of dimple-shape geometry.

duct depth and were assumed to be negligible. The air temperature ($\bar{t}_a$) was determined as an average of the temperatures measured at six central location of the duct cross-section along the flow direction as shown in Fig. 4. The convective heat transfer coefficient was then used to obtain the average Nusselt number from the following expression:

$$\overline{Nu} = \frac{\bar{h}D}{k} \tag{5}$$

The friction factor was determined from the measured values of pressure drop, ΔP, across the test section length, L of 1000 mm as

$$\bar{f}_r = \frac{2\Delta PD}{4\rho Lv^2} \tag{6}$$

The validity of the test setup was verified by conducting experiments for smooth duct under similar conditions. The values of Nusselt number and friction factor determined for smooth duct were compared with the values obtained from correlations of Dittus–Boetler equation for the Nusselt number and modified Blasius equation for the friction factor [30].

Nusse1t number for a smooth rectangular duct is given by Dittus–Boetler equation [30] as

$$Nu_s = 0.023\,Re^{0.8}\,Pr^{0.4}\left(2\frac{R_{av}}{D}\right) \tag{7}$$

Friction factor for a smooth rectangular duct is given by the Modified Blasius equation as

$$f_s = 0.085\,Re^{-0.25} \tag{8}$$

5. Error analysis

An error analysis of experimental measurements has been carried out on the basis of the method proposed by Kline and McClintock [31]. The maximum possible measurement errors in the values of major parameters of present investigation are given below

- Reynolds number = 1.06%
- Heat transfer coefficient = 2.59%
- Nusselt number = 2.78%
- Friction factor = 1.03%

6. Results and discussions

The effect of flow and roughness parameters on heat transfer and friction characteristics for flow of air in a rectangular duct under the present investigation are presented and discussed under this part of the paper.

In order to conduct the validity test of the duct, experimental data were collected on conventional duct having smooth absorbing surface. The average values of Nusselt number and friction factor for the duct having smooth plate were determined.

Figs. 8 and 9 show the comparison of the experimental values of Nusselt and friction factor for roughened solar air heater with those predicted by correlations proposed by Modified Dittus–Boelter correlation for Nusselt number and by Modified-Blasius correlation for friction factor [30]. It can be seen from these figures that the values obtained experimentally are comparable.

Figs. 10 and 11 have been drawn to represent the Nusselt number derived from the test results as a function of the roughness and operating parameters.

Fig. 10 shows the Nusselt number as a function of Reynolds number for relative pitch (p/e) values of 8, 10 and 12 and for a fixed value of relative roughness height (e/D) of 0.0322. The plot is prepared to compare the heat transfer rate for a duct having dimple-shape geometry of different values of relative pitch (p/e). Similar trend has been obtained for Nusselt number for all the values of relative roughness height. It can be seen from the figures that for given values of roughness parameters, the Nusselt number monotonously increases with increase of Reynolds number. It is seen from Fig. 10 that Nusselt number has been found maximum corresponding to relative roughness pitch, (p/e) of 10 which may be discussed on similar lines as investigated by other investigators. Due to separation of the flow at the dimple, reattachment of free shear layer occurs for p/e of 10 and maximum heat transfer coefficient occurs in the vicinity of the reattachment region. For relative roughness pitch (p/e) of 8 and 12 reattachment may not

occur hence the values of heat transfer coefficient correspond to these values of p/e are found to be minimum. Similarly, larger relative roughness height (e/D) might produced more reattachment of free shear layer hence the maximum value of heat transfer is found to be corresponding to relative roughness height (e/D) of 0.0379.

Fig. 11 shows the Nusselt number as a function of Reynolds number for relative roughness height (e/D) values of 0.0189, 0.0289, 0.0322 and 0.0379 and for a fixed value of relative pitch (p/e) of 10. It is seen that Nusselt number increases with increase in relative roughness height, e/D and has been found maximum corresponding to relative roughness height of 0.0379.

Figs. 12 and 13 show the variation in friction factor with Reynolds number for different values of roughness parameters. It is seen from the figures that friction factor decreases monotonously with increase in Reynolds number for different roughness parameters. Fig. 12 shows the friction factor as a function of Reynolds number for relative pitch (p/e) values of 8, 10 and 12 and for a fixed value of relative roughness height (e/D) of 0.0322. The plot is prepared to compare the friction factor for a duct having dimple-shape geometry of different values of relative pitch (p/e). Similar trend has been obtained for friction factor for all the values of relative roughness height. Friction factor has been found minimum for relative roughness pitch corresponding to 10. Similarly Fig. 13 shows the variation of friction factor for relative

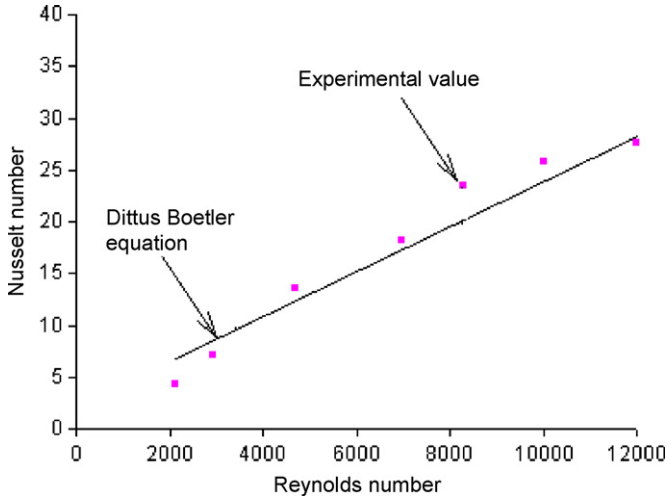

Fig. 8. Comparison of experimental and predicted values of Nusselt number.

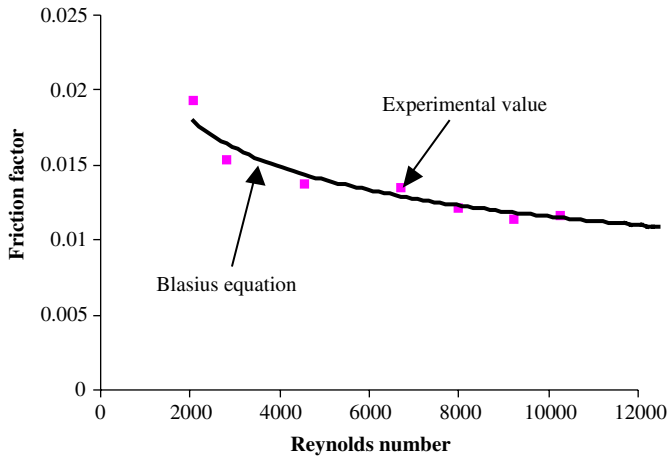

Fig. 9. Comparison of experimental and predicted values of friction factor.

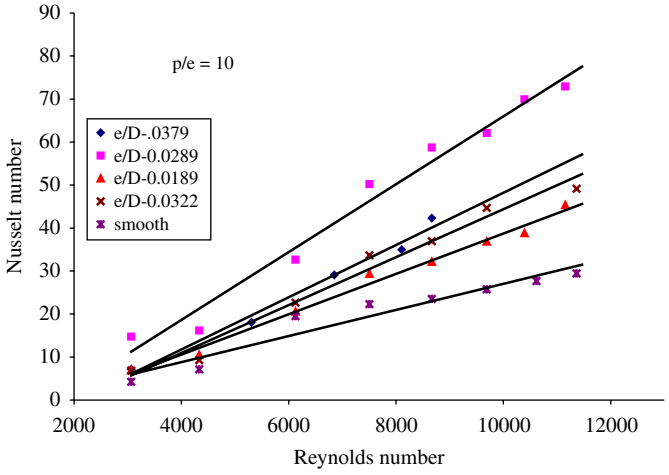

Fig. 11. Variation of Nusselt number with Reynolds number for different values of p/e and for fixed value of e/D.

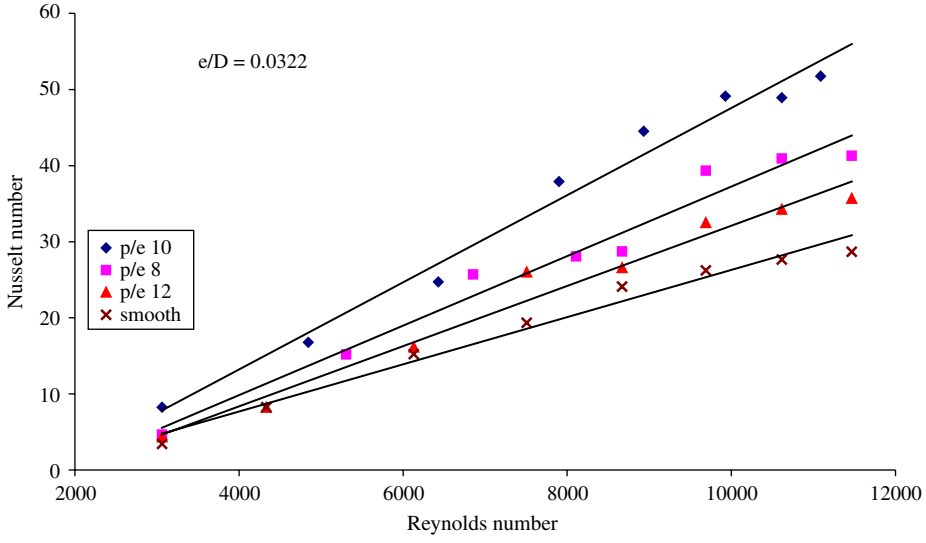

Fig. 10. Variation of Nusselt number with Reynolds number and for different values of e/D and for fixed value of p/e.

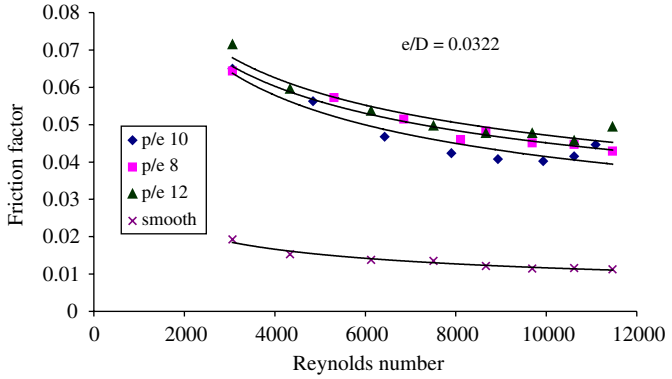

Fig. 12. Variation of friction factor with Reynolds number and for different values of e/D and for fixed value of p/e.

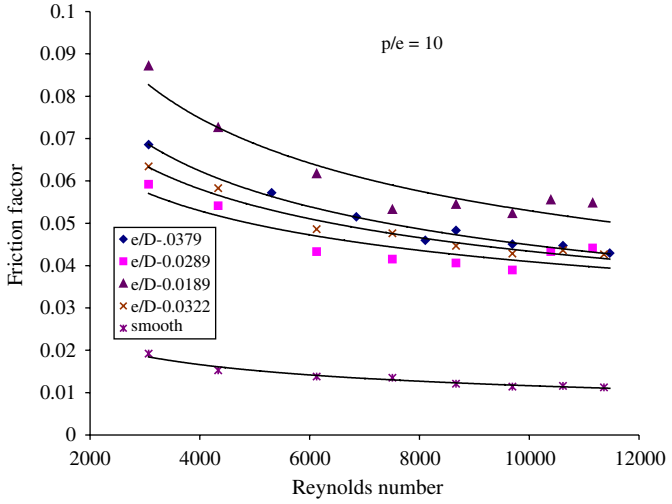

Fig. 13. Variation of friction factor with Reynolds number and for different values of p/e and for fixed value of e/D.

roughness height, e/D of 0.089, 0.0289, 0.0322 and 0.079 and a fix value of p/e of 10. It is seen that friction factor corresponding to relative roughness height, e/D of 0.0189 has been found maximum while friction factor for e/D of 0.0289 is found to be minimum. This may be discussed on the similar lines as discussed above in case of heat transfer coefficient.

7. Correlations for Nusselt number and friction factor

As discussed earlier that the Nusselt number and friction factor are strong functions of flow and roughness parameters, namely flow Reynolds number (Re) and the roughness dimensions of relative pitch (p/e) and relative roughness height (e/D). The functional relationships for Nusselt number and friction factor can therefore be written as

$$Nu = f_n\left(Re, \frac{p}{e}, \frac{e}{D}\right) \tag{9}$$

$$f_r = f_n\left(Re, \frac{p}{e}, \frac{e}{D}\right) \tag{10}$$

7.1. Correlation for Nusselt number

All data points of Nusselt number from experimental data were plotted against Reynolds number as shown in Fig. 14. A regression

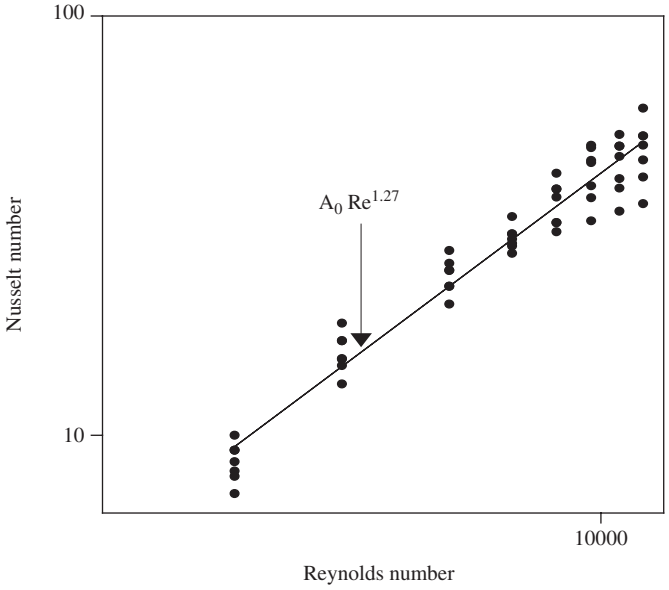

Fig. 14. Plot of Nusselt number versus Reynolds number.

analysis to fit a straight line through these data points may be represented as

$$Nu = A_0(Re)^{1.27} \tag{11}$$

The coefficient A_0 will in fact be a function of other influencing parameters. Now, taking the parameter roughness pitch (p/e) into consideration, the value of $\{(Nu/Re^{1.27}) = A_0\}$ corresponding to all values of (p/e) is plotted against (p/e), as shown in Fig. 15. Regression analysis to fit a second-order quadratic curve fit may be represented by the following expression:

$$\log\left(\frac{Nu}{Re^{1.27}}\right) = \log B_0 + B_1\left(\log\left(\frac{p}{e}\right)\right) + B_2\left(\log\left(\frac{p}{e}\right)^2\right) \tag{12}$$

The Eq. (12) can be rearranged as

$$\left(\frac{Nu}{Re^{1.27}}\right) = B_0\left(\frac{p}{e}\right)^{3.15}\left[\exp(-2.12)\left(\log\left(\frac{p}{e}\right)\right)^2\right] \tag{13}$$

Further, the constant (B_0) will be the function of relative roughness height (e/D).

$$B_0 = \left[\frac{(Nu/Re^{1.27})}{(p/e)^{3.15}[\exp(-2.12)\,(\log(p/e))^2]}\right] \tag{14}$$

Finally, plot for B_0 versus roughness height (e/D) has been drawn as shown in Fig. 16. A second-order quadratic curve fit in the following form is obtained:

$$\log\left[\frac{Nu}{Re^{1.27}}\left(\frac{p}{e}\right)^{3.15}\left[\exp(-2.12)\left(\log\left(\frac{p}{e}\right)\right)^2\right]\right] = \log C_0 + C_1\,\log\left(\frac{e}{D}\right) + C_2\left(\log\left(\frac{e}{D}\right)\right)^2 \tag{15}$$

This can be rewritten as

$$\left(\frac{Nu}{Re^{1.27}}\left(\frac{p}{e}\right)^{3.15}\right)\left[\exp(-2.12)\left(\log\left(\frac{p}{e}\right)\right)^2\right] = C_0\left(\frac{e}{D}\right)^{0.033}\left[\exp(-1.30)\left(\log\left(\frac{e}{D}\right)\right)^2\right] \tag{16}$$

The values of the coefficients are obtained as given below:

$$A_0 = 8.2 \times 10^{-4}, \quad B_0 = 3.1 \times 10^{-4}, \quad C_0 = 1.98 \times 10^{-3}$$

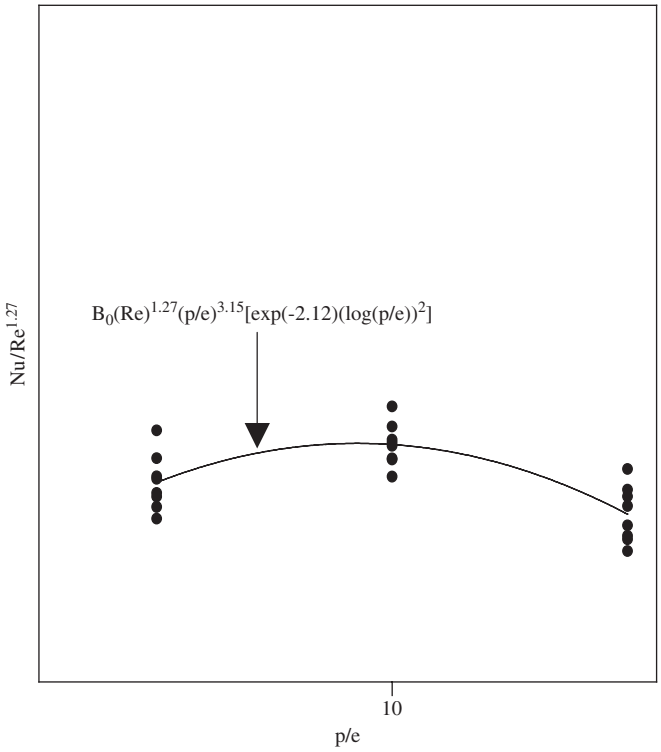

Fig. 15. Plot of $(Nu/Re^{1.27})$ versus (p/e).

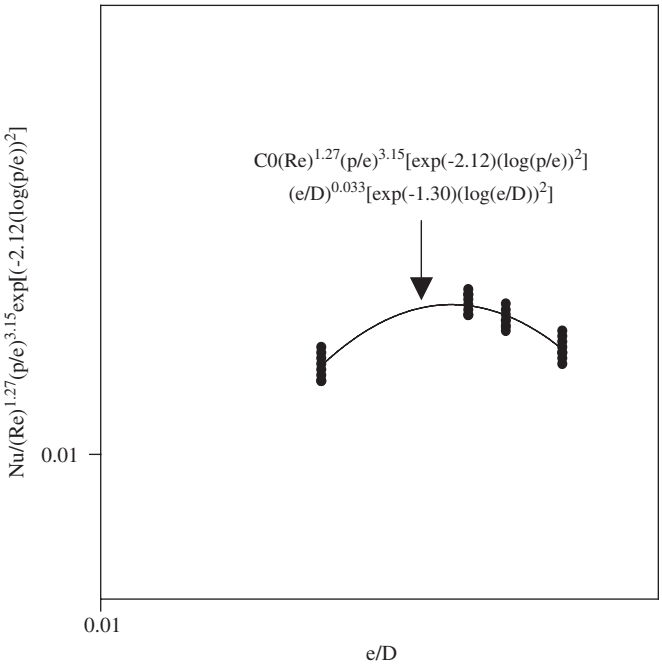

Fig. 16. Plot of $Nu/(Re)^{1.27}(p/e)^{3.15}[\exp(-2.12)(\log(p/e))^2]$ versus (p/e).

These values result in the following correlation for Nusselt numbers:

$$Nu = 5.2\times10^{-4}\,Re^{1.27}\left(\frac{p}{e}\right)^{3.15}\times\left[\exp(-2.12)\left(\log\left(\frac{p}{e}\right)\right)^2\right]\left(\frac{e}{D}\right)^{0.033}\times\left[\exp(-1.30)\left(\log\left(\frac{e}{D}\right)\right)^2\right] \quad (17)$$

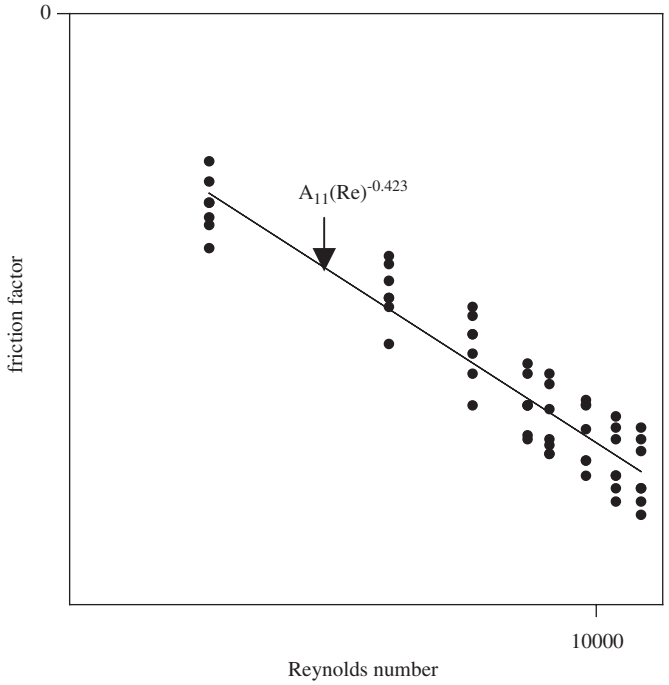

Fig. 17. Plot of friction factor versus Reynolds number.

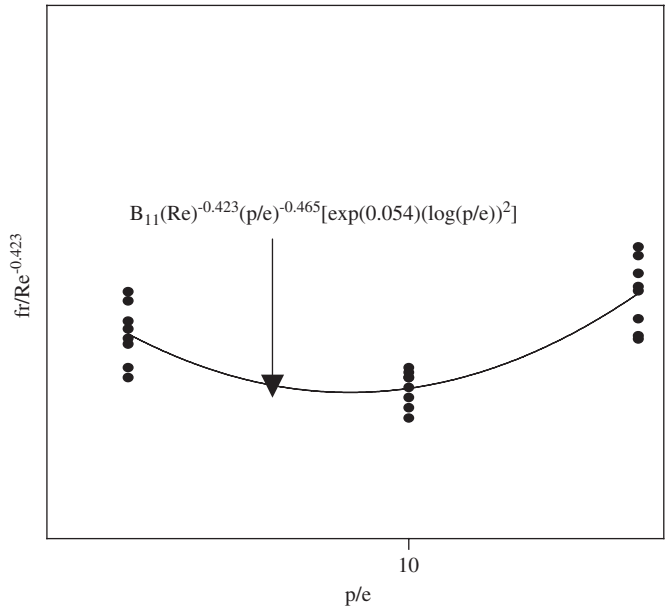

Fig. 18. Plot of $(f_r/Re^{-0.423})$ versus (p/e).

7.2. Correlation for friction factor

A similar procedure has been employed to develop correlation for friction factor as shown in Figs. 17–19. The final form of correlation for friction factor is obtained as follows:

$$f_r = 0.642\,Re^{-0.423}\left(\frac{p}{e}\right)^{-0.465}\left[\exp(0.054)\left(\log\left(\frac{p}{e}\right)\right)^2\right]\times\left(\frac{e}{D}\right)^{-0.0214}\left[\exp(0.840)\left(\log\left(\frac{e}{D}\right)\right)^2\right] \quad (18)$$

Fig. 20 shows the comparison between the experimental values of Nusselt number and those of predicted by the correlation

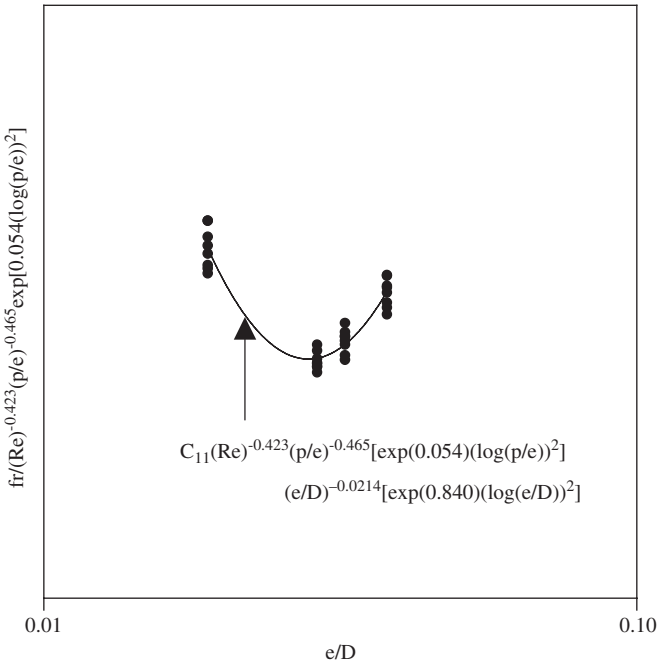

Fig. 19. Plot of $(f_r/Re^{-0.423})(p/e)^{-0.465}[\exp(0.054)(\log(p/e))^2]$ versus (e/D).

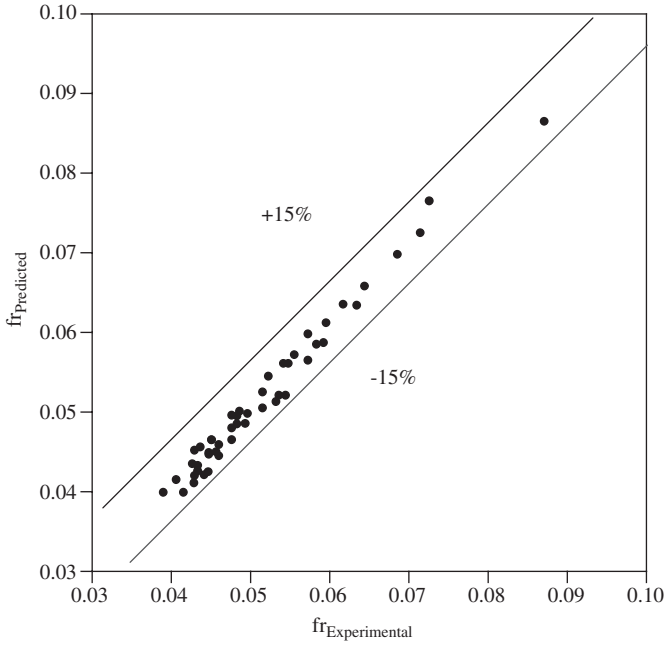

Fig. 21. Comparison of predicted values of friction factor with experimental values.

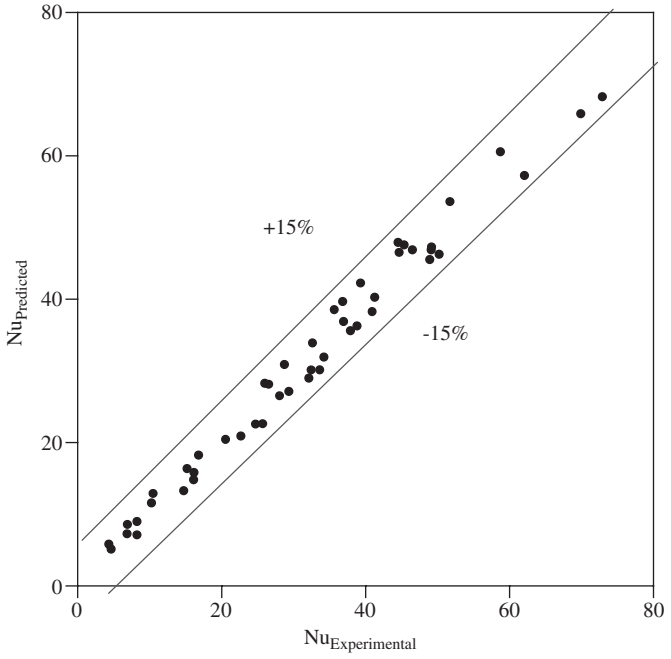

Fig. 20. Comparison of predicted values of Nusselt number with experimental values.

developed for Nusselt number. Fig. 21 shows a comparison of experimental values and the values of friction factor obtained from the developed correlation. The average absolute percentage deviations between the experimental and predicted values have been found to be 7.58 and 4.68 for Nusselt number and friction factor, respectively.

8. Conclusions

An extensive experimental study has been carried out to predict the heat transfer and flow characteristics of a solar air heaters having roughened duct provided dimple-shape roughness geometry as artificial roughness. It can be concluded that heat transfer can be enhanced considerably as a result of providing dimple-shape roughness geometry on the absorber plate of a solar air heater duct. Nusselt number and friction factor are the strong function of the system and operating parameters.

The maximum value of Nusselt number has been found corresponds to relative roughness height (e/D) of 0.0379 and relative pitch (p/e) of 10. While minimum value of friction factor has been found correspond to relative roughness height (e/D) of 0.0289 and relative pitch (p/e) of 10. It is therefore, roughness parameters of the geometry can be selected by considering the net heat gain and corresponding power required to propel air through the duct. Further different arrangement mode of the dimple-shape artificial roughness on the absorbing plate may be investigated in order to get the optimal arrangement mode of such artificial roughness.

Based on experimental data collected during investigation, correlations for Nusselt number and friction factor have been developed for the investigated system. These correlations developed for such systems have been found to predict the values of Nusselt number and friction factor reasonably well under the given range of parameters.

References

[1] Han JC. Heat transfer and friction characteristics in rectangular channels with rib turbulators. ASME J Heat Transfer 1988;110:321–8.
[2] Han JC. Heat transfer and friction in channels with two opposite rib-roughened walls. ASME J Heat Transfer 1984;106:774–81.
[3] Han JC, Glicksman LR, Rohsenow WM. An investigation of heat transfer and friction for rib-roughened surfaces. Int J Heat Mass Transfer 1978;21:1143–56.
[4] Han JC, Park JS, Lei CK. Heat transfer enhancement in channels with turbulence promoters. ASME J Eng Gas Turbines Power 1985;107:628–35.
[5] Han JC, Zhang YM, Lee CP. Augmented heat transfer in square channels with parallel, crossed and V-shaped angled ribs. ASME J Heat Transfer 1991;113:590–6.
[6] Lau SC, Kukreja RT, McMillin RD. Effects of V-shaped rib arrays on turbulent heat transfer and friction of fully developed flow in a square channel. Int J Heat Mass Transfer 1991;34:1605–16.
[7] Lau SC, McMillin RD, Han JC. Turbulent heat transfer and friction in a square channel with discrete ribs turbulators. ASME J Turbomach 1991;113:360–6.

[8] Lau SC, McMillin RD, Han JC. Heat transfer characteristics of turbulent flow in a square channel with angled discrete ribs. ASME J Turbomach 1991;113: 367–74.
[9] Taslim ME, Bondi LA, Kercher DM. An experimental investigation of heat transfer in an orthogonally rotating channel roughened with 45 deg. Criss-cross ribs on two opposite walls. ASME J Turbomach 1991;113:346–53.
[10] Taslim ME, Li T, Kercher DM. Experimental heat transfer and friction in channels roughened with angled, V-shaped, and discrete ribs on two opposite walls. ASME J Turbomach 1996;118:20–8.
[11] Liou TM, Hwang JJ. Effect of ridge shapes on turbulent heat transfer and friction in a rectangular channel. Int J Heat Mass Transfer 1993;36:931–40.
[12] Han JC, Park JS. Developing heat transfer in rectangular channels with rib turbulators. Int J Heat Mass Transfer 1988;31:183–95.
[13] Prasad K, Mullick SC. Heat transfer characteristics of a solar air heater used for drying purposes. Appl Energy 1983;13:83–93.
[14] Gupta D. Investigations on fluid flow and heat transfer in solar air heaters with roughened absorbers. Ph.D. thesis, University of Roorkee, India, 1993.
[15] Saini RP, Saini JS. Heat transfer and friction factor correlations for artificially roughened ducts with expanded metal mesh as roughness element. Int J Heat Mass Transfer 1997;40:973–86.
[16] Karwa R. Investigation of thermo-hydraulic performance of solar air heaters having artificially roughened absorber plate. Ph.D. thesis, University of Roorkee, India, 1997.
[17] Jaurker AR, Saini JS, Gandhi BK. Heat transfer and friction characteristics of rectangular solar air heater duct using rib-grooved artificial roughness. Solar Energy 2006;80(8):895–907.
[18] Bhagoria JL, Saini JS, Solanki SC. Heat transfer coefficient and friction factor correlations for rectangular solar air heater duct having transverse wedge shaped rib roughness on the absorber plate. Renew Energy 2002;25(3):341–69.
[19] Chaube A, Sahoo PK, Solanki SC. Analysis of heat transfer augmentation and flow characteristics due to rib roughness over absorber plate of a solar air heater. Renew Energy 2006;31(3):317–31.
[20] Verma SK, Prasad BN. Investigation for the optimal thermohydraulic performance of artificially roughened solar air heaters. Renew Energy 2000; 20(1):19–36.
[21] Gupta D, Solanki SC, Saini JS. Thermohydraulic performance of solar air heaters with roughened absorber plates. Solar Energy 1997;61(1):33–42.
[22] Mittal MK, Varun, Saini RP, Singal SK. Effective efficiency of solar air heaters having different types of roughness elements on the absorber plate. Energy 2007;32(5):739–45.
[23] Varun, Saini RP, Singal SK. A review on roughness geometry used in solar air heaters. Solar Energy 2007;81(11):1340–50.
[24] Chukin AV, Koslov AP, Agachev RS. Study and Application of hemispherical cavities for surface heat transfer augmentation. In: ASME 40th international gas turbine and aero congress, No. 95-GT-59, Houston, 1995.
[25] Chyu MK, Yu Y, Ding H, Downs JP, Soechting F. Concavity enhanced heat transfer in an internal cooling passage. In: ASME 42nd international gas turbine and aero congress, ASME paper no. 97-GT-437, Orlando, FL, 1997.
[26] Lin YL, Shih TIP, Chyu MK. Computations of flow and heat transfer in a channel with rows of hemispherical cavities. In: ASME Turbo Expo, ASME 99-GT-263, Indianapolis, 1999.
[27] Moon HK, O'Connell T, Glezer B. Channel height effect on heat transfer and friction in a dimpled passage. In: ASME Turbo Expo, ASME 99-GT-163, Indianapolis, 1999.
[28] Mahmood GI, Hill ML, Nelson DL, Ligrani PM, Moon HK, Glezer B. Local heat transfer and flow structure on and above a dimpled surface in a channel.
[29] ASHRAE Standard 93–97, Methods of testing to determine the thermal performance of solar collectors, 1997.
[30] Han JC, Park JS, Lei CK. Heat transfer enhancement in channels with turbulence promoters. Trans ASME J Eng Gas Turbines Power 1985;107: 628–35.
[31] Kline SJ, Mcclintock FA. Describing uncertainties in single sample experiments. Mech Eng 1953;75:3–8.